JACS
JOURNAL OF THE AMERICAN CHEMICAL SOCIETY
Article
pubs.acs.org/JACS

Chiral Effect at Protein/Graphene Interface: A Bioinspired Perspective To Understand Amyloid Formation

Guangyan Qing,*[,†,‡] Shilong Zhao,[‡] Yüting Xiong,[‡] Ziyu Lv,[‡] Fenglei Jiang,[§] Yi Liu,[§] Hui Chen,[‡] Mingxi Zhang,[‡] and Taolei Sun*[,†,‡]

[†]School of Chemistry, Chemical Engineering and Life Science, Wuhan University of Technology, 122 Luoshi Road, Wuhan 430070, People's Republic of China

[‡]State Key Laboratory of Advanced Technology for Materials Synthesis and Processing, Wuhan University of Technology, 122 Luoshi Road, Wuhan 430070, People's Republic of China

[§]College of Chemistry and Molecular Sciences, Wuhan University, Wuhan 430072, People's Republic of China

Supporting Information

ABSTRACT: Protein misfolding to form amyloid aggregates is the main cause of neurodegenerative diseases. While it has been widely acknowledged that amyloid formation *in vivo* is highly associated with molecular surfaces, particularly biological membranes, how their intrinsic features, for example, chirality, influence this process still remains unclear. Here we use cysteine enantiomer modified graphene oxide (GO) as a model to show that surface chirality strongly influences this process. We report that *R*-cysteine modification suppresses the adsorption, nucleation, and fiber elongation processes of Aβ(1−40) and thus largely inhibits amyloid fibril formation on the surface, while *S*-modification promotes these processes. And surface chirality also greatly influences the conformational transition of Aβ(1−40) from α-helix to β-sheet. More interestingly, we find that this effect is highly related to the distance between chiral moieties and GO surface, and inserting a spacer group of about 1−2 nm between them prevents the adsorption of Aβ(1−40) oligomers, which eliminates the chiral effect. Detailed study stresses the crucial roles of GO surface. It brings novel insights for better understanding the amyloidosis process on surface from a biomimetic perspective.

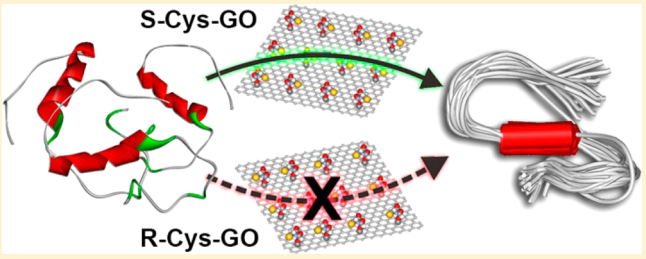

1. INTRODUCTION

Protein amyloidosis is associated with many neurodegenerative diseases, such as, Alzheimer's and Parkinson's diseases.[1−4] Recently, more and more evidence has pointed to the fact that molecular surfaces, particularly biological membranes, play crucial roles in this process.[5−10] It has been pointed out that key procedures of protein amyloidosis *in vivo*, including sequential APP cleavage by β-secretase and γ-secretase to form Aβ precursors, deposition, and aggregation of Aβ after misfolding to form plaques may mainly occur on cell membranes[11−19] (Scheme 1A). From a viewpoint of chemistry, cell membranes are composed of phospholipid bilayers with proteins integrated into them.[20] As an amphiphilic molecule bearing a hydrophilic head and a hydrophobic tail, a natural phospholipid is a chiral molecule showing very high preference to the L-enantiomer. And highly ordered arrangement of them endows the membrane with an apparent asymmetric feature, which is one of the predominant biochemical signatures of life.[21−23] In previous works, we and others have shown that chirality remarkably influences protein adsorption dynamics[24−26] and subsequent cell behaviors[27,28] on surfaces. This inspires us to introduce surface chirality into the study of amyloid formation from a biomimetic point of view.

As a kind of emerging two-dimensional atomic material, besides other advantages like high mechanical stiffness and good electrical and thermal conductivity,[29] chemically modified graphene, especially graphene oxide (GO), also possesses distinct amphiphilic properties[30−32] similar to cell membranes. It allows interactions with cell membranes and excellent ability to pass through the blood−brain barrier,[33−35] which brings broad application prospects for this kind of material in biology and medicine.[36,37] On the other hand, the *in vivo* concentration of dissociated Aβ peptides is normally far lower than its critical micelle concentration, and it has been shown that they incline to adsorb and aggregate strongly on a graphene surface,[38,39] which may largely accelerate the fibrillation process. These properties indicate that GO can act as an ideal platform to investigate the chiral effect for amyloid formation on surfaces, when it is combined with chiral characteristics (Scheme 1B). For this purpose, we developed a series of chiral GO materials through chemical modification with *R*(*S*)-cysteine and derivatives. We show that *R*-cysteine modified GO (*R*-Cys-GO) largely suppresses the adsorption, nucleation, and fiber

Received: May 18, 2014
Published: July 10, 2014

   dx.doi.org/10.1021/ja5049626 | J. Am. Chem. Soc. 2014, 136, 10736−10742

Scheme 1. (A) Cell Membranes Play a Crucial Role in Protein Amyloidosis *in Vivo*, Wherein Several Key Procedures for Amyloid Formation, for example, APP Cleavage and Oligomer Aggregation, Mainly Occur on Them, and (B) Chiral Nature of Phospholipid Double Layer Inspires Us To Introduce Chirality into the Study of Amyloid Formation on Surface, in Which Graphene Is Used As an Ideal Platform To Perform This Research

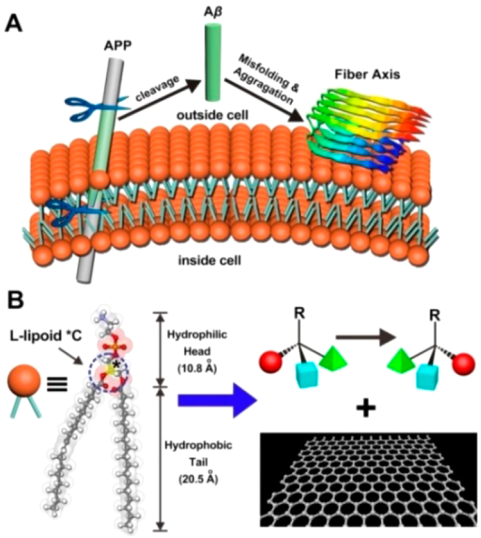

elongation processes of Aβ(1−40) and thus significantly inhibits amyloid fibril formation on the surface; while *S*-cysteine modified GO (*S*-Cys-GO) promotes these processes. And surface chirality also greatly influences the conformational transition of Aβ(1−40) from α-helix to β-sheet. More interestingly, we find that this effect is highly related to the distance between chiral moieties and GO surface, and inserting a spacer group of about 1−2 nm between them prevents the adsorption of Aβ(1−40) oligomers, which eliminates the chiral effect. Detailed study indicates that the surface plays a crucial role in this effect, which not only enables local enrichment of Aβ(1−40) oligomers but also mediates the stereoselective interaction between chiral moieties and peptide. This finding presents a new perspective to better understand how biological membranes participate in amyloid formation.

2. RESULTS AND DISCUSSION

R(*S*)-Cysteine molecules possess a carboxylic group and a thiol group, both of which are good hydrogen bonding (H-bonding) donors capable of interacting with Aβ peptides. It is worth noting that the natural L-cysteine possesses *R*-stereoconfiguration, which is opposite to other amino acids. Three pairs of reference compounds (Scheme 2) were also designed to clarify the roles of these groups. In the first one, (*R*(*S*)-ECys), the carboxylic group of cysteine has been esterified, while in the second, the thiol group has been methylated (*R*(*S*)-MCys). In the third (*R*(*S*)-DCys), a long chain of spacer group was introduced between the cysteine moiety and GO to study the distance factor for the chiral effect (according to a model calculation, the vertical distance between the top carboxylic group and the GO surface is approximately 16 Å, in comparison with about 6 Å for *R*(*S*)-Cys-GO). The enantiomers of these molecules were immobilized on the GO surface through a typical condensation reaction with high efficiency.[40−42] Corresponding characterization data indicated that these

Scheme 2. Illustration of Molecular Structures of GO Modified with *R*(*S*)-Cysteine (*R*(*S*)-Cys-GO), Esterified *R*(*S*)-Cysteine (*R*(*S*)-ECys-GO), Sulfur-Methylated *R*(*S*)-Cysteine (*R*(*S*)-MCys-GO), and Diethylene Glycol Modified *R*(*S*)-Cysteine (*R*(*S*)-DCys-GO)

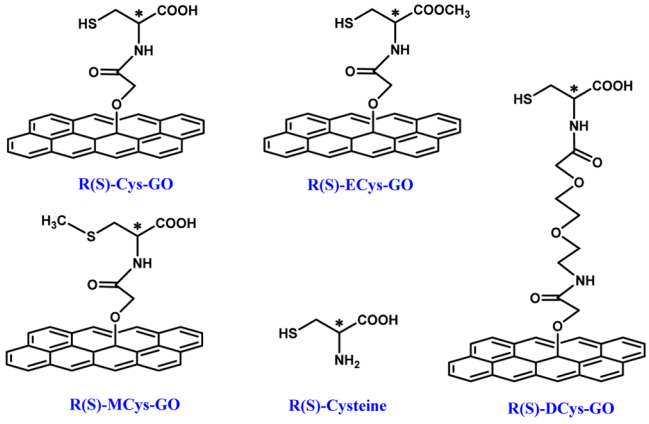

enantiomers were identical in chemical compositions and other properties, for example, graft density (approximately one cysteine molecule in five to six aromatic rings in GO, calculated from the atomic ratios measured by XPS), and ζ potential, as shown in Figures S1−S7 in Supporting Information.

The fibrillation process of Aβ peptides can mainly be divided into nucleation and elongation phases,[43−46] as shown in Figure 1A. We first studied the influence of chiral-modified GO on the nucleation phase of Aβ(1−40). In this experiment, various GO samples (0.15 mg·mL^{-1}) were added to Aβ(1−40) solution (25 μmol·L^{-1}) at the beginning of incubation at 37 °C, and then the rates of amyloid formation were evaluated using a standard thioflavine-T (ThT) binding assays.[47,48] Figure 1B shows the growth curves of Aβ(1−40) in the absence and presence of *R*(*S*)-Cys-GO. Without chiral samples (black curve), Aβ(1−40) began to aggregate at the 24 h and completely fiberized after the 38th hour, resulting in a half growth cycle of 7 h. The addition of *R*-Cys-GO remarkably postponed this process for about 11 h (red curve), while *S*-Cys-GO brought forward this process nearly 12 h (blue curve). This indicates that *R*-Cys-GO largely suppressed the nucleation of Aβ(1−40), while *S*-Cys-GO accelerated this process.

To study their influence on the fiber elongation phase, chiral-modified GO was added (0.15 mg·mL^{-1}) to peptide solution after about 10 h of incubation at 37 °C to allow the formation of oligomers, simultaneously with the addition of ThT. The corresponding growth curves are shown in Figure 1C. After adding *R*-Cys-GO (red curve), fluorescent intensity did not change obviously before 32nd hour and started to increase only slightly after that. However, for *S*-Cys-GO (blue curve), the fluorescent intensity remarkably increased immediately after its addition. Lower concentrations (e.g., 0.1 mg·mL^{-1}) of *R*(*S*)-Cys-GO gave similar results, while the difference was a little smaller (Figure S8B in Supporting Information). It shows that *R*-Cys-GO can also inhibit the fiber elongation process of Aβ(1−40).

Similarly, *R*- and *S*-ECys-GO also show different influence on the fibrillation of Aβ(1−40) at both the nucleation and elongation phases, but the effect is significantly weaker than that for *R*(*S*)-Cys-GO, as typically shown in Figure 1D for the nucleation phase (red and blue curves). However, for *R*(*S*)-MCys-GO, in which the thiol group has been methylated, the

dx.doi.org/10.1021/ja5049626 | J. Am. Chem. Soc. 2014, 136, 10736−10742

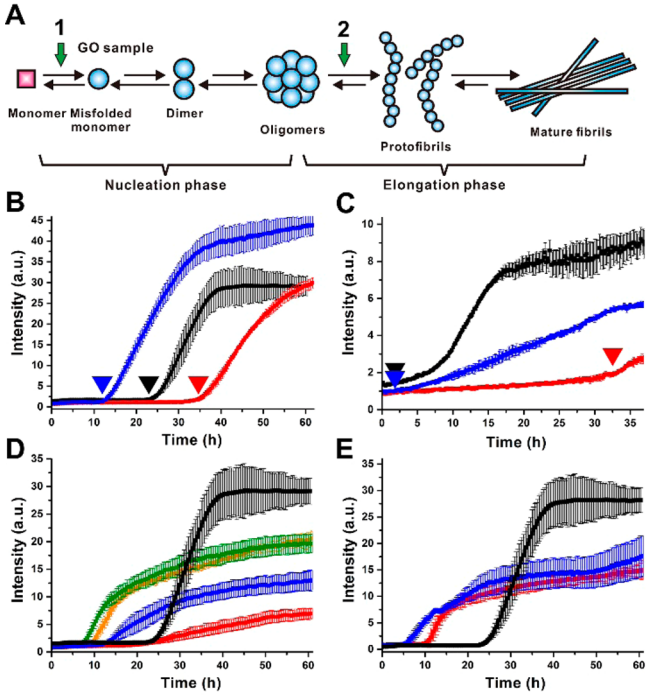

Figure 1. Influence of chiral-modified GO on the fibrillation process of Aβ(1−40). (A) Fibrillation of Aβ peptides can be divided into nucleation phase to form oligomers and elongation phase to form fibers.[43] (B) *R*- (red) and *S*-Cys-GO (blue) added at the beginning of incubation. (C) *R*- (red) and *S*-Cys-GO (blue) added after 10 h of incubation. (D) *R*- (red) and *S*-ECys-GO (blue), and *R*- (orange) and *S*-MCys-GO (green) added at the beginning of incubation. (E) *R*- (red) and *S*-DCys-GO (blue) added at the beginning of incubation. Black curves are all the control experiment with only Aβ(1−40) peptides. In all panels, error bars show the standard deviations of the averaged data sets. Experiments were repeated three times, and each time the experiment was carried out in triplicate.

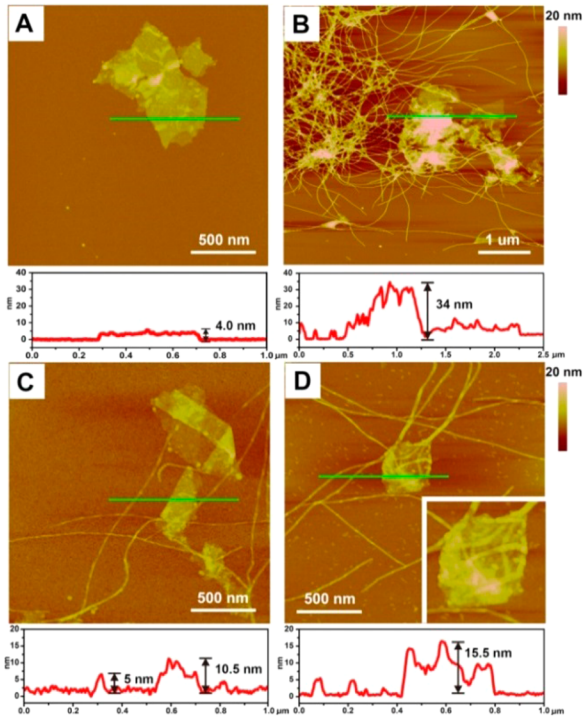

Figure 2. AFM images of *R*(*S*)-Cys-GO after incubation in Aβ(1−40) solutions: (A, C) *R*-Cys-GO; (B, D) *S*-Cys-GO; (A, B) *R*(*S*)-Cys-GO were added at the beginning of incubation; (C, D) GO samples were added after 10 h of incubation at 37 °C.

difference is rather small (green and orange curves in Figure 1D). This indicates that carboxylic and thiol groups may play a crucial role in the stereoselective interaction with Aβ(1−40), which has been proven by results of two-dimensional ^{1}H nuclear magnetic resonance (NMR) spectroscopies shown later. For *R*- and *S*-DCys-GO, unexpectedly, the difference between growth curves of Aβ(1−40) was also slight in both the nucleation (Figure 1E) and elongation phases (Figure S8E in Supporting Information), although the exposed groups are the same as *R*(*S*)-Cys-GO. Moreover, in a control experiment without the participation of GO, we found that the addition of *R*- or *S*-cysteine had no influence on the fibrillation process (Figure S8D in Supporting Information). This points to an interesting deduction that the chiral effect may require the synergy of stereoselective interactions contributed by chiral moieties, and the participation of GO surface, and the synergy may be confined to a very narrow spatial range near the surface within 1−2 nm. We also used other amino acids (e.g., serine and tyrosine) to do the experiments (Figure S9 in Supporting Information), but the chiral effect was not as distinct as that of cysteine.

To better understand this effect, we then tracked the fibrillation of Aβ(1−40) on *R*(*S*)-Cys-GO surfaces using atom force microscopy (AFM).[49] Figure 2A,B shows AFM images of *R*- and *S*-Cys-GO surface (0.15 mg·mL^{-1}) after incubation in Aβ(1−40) monomer solution (25 μmol·L^{-1}) for 30 h at 37 °C. Interestingly, the *R*-Cys-GO surface was rather clean, and long fibers could not be observed on it. Only a small amount of short oligomers was adsorbed on it, resulting in a slight increase of the maximum height for the GO layer from 4 nm (double-layer GO) to 6 nm. This phenomenon well supports the result mentioned above that *R*-Cys-GO inhibited the fibrillation process. By comparison, a great quantity of long fibers were found on *S*-Cys-GO surface (Figure 2B), which interlinked with each other and accumulated on the GO surface to form a fiber network. The maximum height of the GO layer dramatically increased to 34 nm due to the multilayer accumulation of fibers, which is about eight times higher than surrounding single fibers (approximately 4 nm). We noticed that many long fibers spread out from the GO surface and covered both sides of GO. This indicates that *S*-Cys-GO has strong complexation with Aβ(1−40), which greatly accelerated the fibrillation.

In another experiment, *R*(*S*)-Cys-GO was added to Aβ(1−40) solution after 10 h of incubation at 37 °C to study the elongation phase. Figure 2C,D shows AFM images of *R*(*S*)-Cys-GO surfaces after further incubation for 10 h. A control experiment without GO samples indicated that a considerable amount of long fibers had already formed under these conditions (Figure S10B in Supporting Information). By comparison, the amount of long fibers formed after incubation was much less with the addition of *R*- and *S*-Cys-GO. This is consistent with the growth curves shown in Figure 1C that the fluorescent intensities in both cases were obviously lower than the control experiment without GO samples. However, the difference between *R*- and *S*-surfaces was still remarkable. As shown in Figure 2D, long fibers forming in solution adhered firmly to *S*-Cys-GO in a multilayer accumulation fashion, resulting in a maximum height of about 15.5 nm. This further proves that *S*-Cys-GO has strong complexation with Aβ(1−40).

dx.doi.org/10.1021/ja5049626 | J. Am. Chem. Soc. 2014, 136, 10736−10742

Nevertheless, for *R*-Cys-GO (Figure 2C), it seems that the fibers were just "put" randomly on the surface, lacking firm association with it. This indicates that the interaction between fibers and the *R*-surface is much weaker than that with *S*-surface.

Quartz crystal microbalance (QCM) was further used to study the adsorption behaviors of Aβ(1−40) monomers and oligomers on *R*(*S*)-Cys-GO surfaces.[50−52] In this experiment, *R*(*S*)-Cys-GO coated quartz crystals were obtained by an assembly process via the reaction between thiol groups of cysteine on one side of GO and the gold layer on crystals, leaving cysteine moieties on the other side of GO free to interact with Aβ(1−40) (inset in Figure 3A). Aβ(1−40)

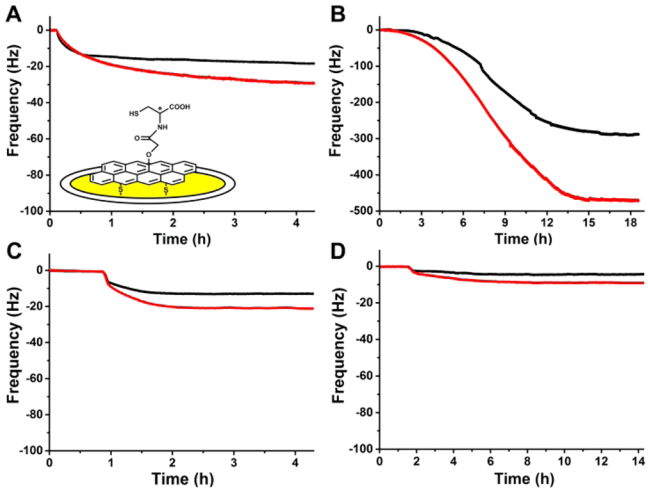

Figure 3. Time dependence of frequency change of QCM crystals with *R*(*S*)-Cys-GO (A, B) and *R*(*S*)-DCys-GO (C, D) upon adsorption of Aβ(1−40) monomers (A, C) and oligomers (B, D). Black and red curves are all *R*- and *S*-surfaces, respectively. The adsorption quantities (*A*) were calculated according to the equation: $A = \Delta F \times 17.7/n$, ng·cm^{-2}, where *n* is the overtone number.

monomers (Figure 3A) exhibited distinctly stronger adsorption on *S*-Cys-GO surface than *R*-Cys-GO surface, inducing frequency change (ΔF) of quartz crystals of 29.0 and 16.2 Hz, corresponding to adsorption quantities of 171.5 and 95.7 ng·cm^{-2}, respectively. Aβ(1−40) oligomers (Figure 3B) showed much stronger adsorption on both *R*- and *S*-surfaces, and the difference between them was also larger (adsorption quantity 2.78 × 10^3 ng·cm^{-2} for *S*-surface, 1.69 × 10^3 ng·cm^{-2} for *R*-surface). In the experiments with *R*(*S*)-DCys-GO (Figure 3C,D for monomers and oligomers, respectively), though similar chiral discrimination effect was observed, the adsorption quantities for oligomers on both surfaces were much lower, which decreased to about 1/50 of those on *R*(*S*)-Cys-GO modified crystals.

In a control experiment, in which *R*- and *S*-cysteine were directly grafted onto quartz crystals via amide bonds (thiol and carboxylic groups were exposed outside to mimic *R*(*S*)-Cys-GO), the adsorption quantities for Aβ(1−40) monomers on *R*(*S*)-Cys surfaces were slightly larger than those on *R*(*S*)-Cys-GO surfaces. However, these values were much lower for oligomers (ΔF < 10 Hz) and the difference between *R*- and *S*-surfaces were also small (see Figure S11 in Supporting Information). All these data indicate the crucial role of GO surface in this chiral effect. GO significantly promoted the adsorption of Aβ(1−40) monomers and oligomers. Due to the amphiphilic nature of GO, hydrophobic oligomers are apt to adsorb on it via hydrophobic and $\pi-\pi$ interactions, exhibiting a much higher adsorption quantity than monomers. This behavior is quite similar to that of cell membranes, which are also amphiphilic. However, upon introduction of a spacer group between chiral moieties and the surface, for example, *R*(*S*)-DCys, Aβ(1−40) oligomers could not interact directly with GO surface, which, therefore, showed very low adsorption quantities.

On the other hand, isothermal titration calorimetry (ITC)[53−56] was used to investigate the binding behaviors between Aβ(1−40) and *R*(*S*)-Cys-GO, as shown in Figure 4A.

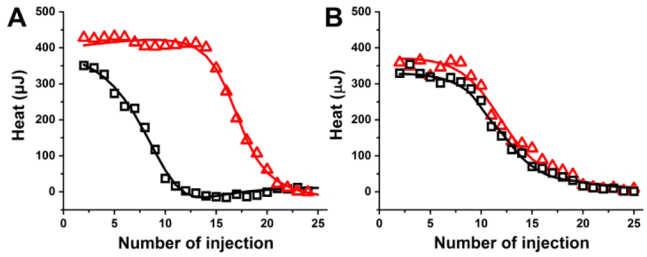

Figure 4. Heat effects associated with the injections of *R*(*S*)-Cys-GO (A) or *R*(*S*)-DCys-GO (B) into Aβ(1−40) solutions at 25 °C: (□) *R*-samples; (△) *S*-samples. The solid lines represent the simulation results from the data of titration using the NanoAnalyze software.

Both *R*- and *S*-Cys-GO were inclined to complex with Aβ(1−40) in a two-stage mode (confirmed by the results of nonlinear curve fitting), but their binding behaviors were quite different. For *R*-Cys-GO, it exhibited strong binding with Aβ(1−40) in the first stage, accompanying a sharp decrease of heat before the 12th injection, while the strong binding between *S*-Cys-GO and Aβ(1−40) occurred at the second stage. Though direct calculation of the binding constants is not accessible due to the unknown concentrations of GO in a molar unit, it can be reasonably inferred that the complexation of Aβ(1−40) with *S*-Cys-GO (ΔH −431 μJ) is stronger than that with *R*-Cys-GO (ΔH −365.9 μJ). More interestingly, no evident difference was observed between the binding isotherms (Figure 4B) for *R*- and *S*-DCys-GO with Aβ(1−40), indicating similar binding behaviors. These results were consistent with the QCM experiment (Figure 2) and the growth curves shown in Figure 1, which verified the great influence of a spacer group on the chiral effect from a thermodynamic point of view.

The conformational transition from α-helix to β-sheet is the foundation for oligomer formation and further fibrillation.[57−59] We also monitored the influence of *R*(*S*)-Cys-GO on this process using circular dichroism (CD) spectra. In this experiment, the concentrations of both Aβ(1−40) and *R*(*S*)-Cys-GO were twice of those used in Figure 1, because the fibrillation process is too slow, which may bring difficulty to observation. For pure Aβ(1−40) peptide (Figure S12 in Supporting Information), the intensity of α-helix peak[60] near 200 nm decreased gradually with the increase of incubation time, which vanished almost completely after 84 h. Since the CD signal of β-sheet (a broad peak at about 210−220 nm) is very weak, it appeared at the 120th hour of incubation. And *R*(*S*)-Cys-GO did not show obvious signals in range of 190−250 nm (Figure 5A). The addition of *S*-Cys-GO accelerated the decrease of the α-helix peak, which vanished at the 48th hour, and obvious signals of β-sheet appeared at the 96th hour (Figure 5C). However, interestingly, *R*-Cys-GO addition largely

dx.doi.org/10.1021/ja5049626 | J. Am. Chem. Soc. 2014, 136, 10736−10742

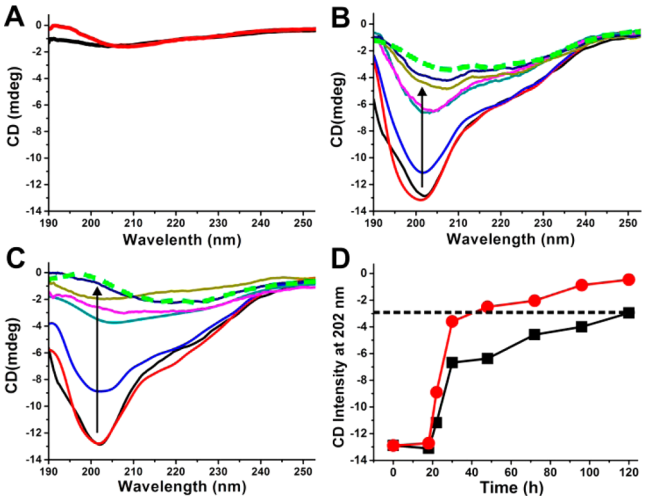

Figure 5. (A) CD spectra for *R*- (black) and *S*-Cys-GO (red). (B, C) Changes of CD spectra of Aβ(1−40) with addition of *R*- (B) or *S*-Cys-GO (C). Black, 0 h; red, 18 h; blue, 22 h; olive, 30 h; purple, 48 h; dark yellow, 72 h; navy, 96 h; green dash, 120 h. (D) Comparison of CD intensities for α-helix peak (202 nm) dependent on time with *R*- (black) and *S*-Cys-GO (red).

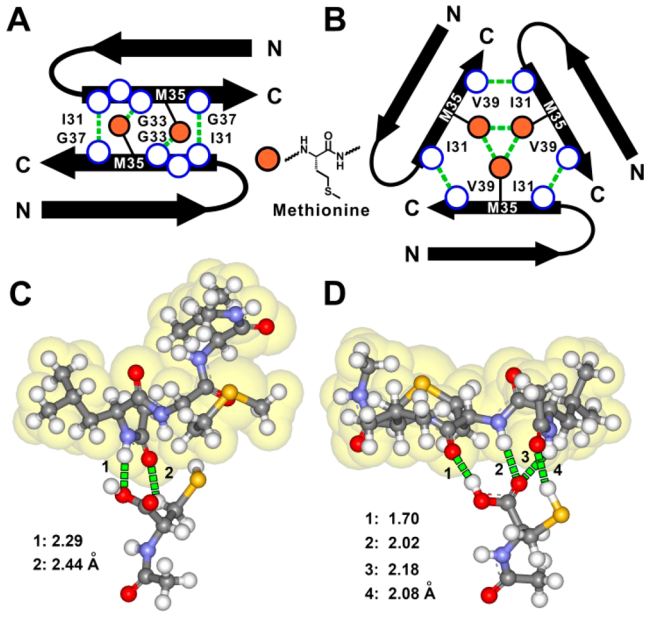

Figure 6. (A, B) Two possible self-assembly mechanisms contributing to Aβ(1−40) amyloidosis,[61−63] showing the critical sequence of Met35. (C, D) Interaction models of tripeptide LMV with *R*-NA-Cys (C) and *S*-NA-Cys (D). Hydrogen bonds are indicated by green dotted lines.

suppressed this process (Figure 5B). The intensity of the α-helix peak decreased obviously more slowly, which retained about 35% after 72 h of incubation. As a result, the CD spectrum of Aβ(1−40) with *R*-Cys-GO at the 120th hour was quite similar to that with *S*-Cys-GO at the 48th hour. Figure 5D is a comparison of intensity change for the α-helix peak (202 nm) dependent on time with the presence of *R*- and *S*-Cys-GO. If we correlate it with the nucleation and fiber elongation phases of fibrillation, we can find that these results are very well consistent with the AFM and QCM experiments, which leads to a conclusion that the chiral effect on fibrillation may be highly related to different influences on Aβ(1−40) conformations.

Tycko and co-workers proposed two assembly modes through data analysis from solid-state NMR in 2006[61] and 2008.[62] They pointed out that the 35th amino acid, methionine (M35, orange balls in Figure 6A) is the key sequence to induce aggregation, which has been recognized as an important target for the design of anti-Alzheimer's drugs. It can form a compact H-bonding interaction with neighboring G33 in another peptide (Figure 6A), or self-assemble to form a trimer structure (Figure 6B). Based on this knowledge, we chose a short tripeptide fragment,[64] Leu-Met-Val (LMV), to simulate the binding site of Aβ(1−40) peptide and investigated its stereoselective interaction with *R*(*S*)-cysteine moieties (*N*-acetyl-*R*(*S*)-cysteine, *R*(*S*)-NA-Cys, was used here to simulate *R*(*S*)-Cys-GO). We first used quantum chemistry calculation (Gaussian, density function theory at 6-311G level) to figure out the optimized interaction models as shown in Figure 6C,D. LMV revealed four sets of strong H-bonds with the carboxylic and thiol groups of *S*-NA-Cys (Figure 6D), while only two sets of relatively weaker H-bonds were found with the carboxylic group of *R*-NA-Cys (thiol group did not participate into the interaction, Figure 6C).

The stereoselective interaction was further proven by experiments. A fluorescent titration experiment[65,66] revealed an association constant (K_a) of 8.06×10^4 L·mol^{-1} when LMV interacted with *S*-NA-Cys, which is about 120 times higher than that with *R*-NA-Cys. As shown in Figure 7A,B, fluorescence of fluorescein-labeled LMV solution was completely quenched by *R*-NA-Cys, while *S*-NA-Cys only induced a decrease of about 12%. On the other hand, in the study of two-dimensional ^{1}H−^{1}H COSY NMR spectroscopy,[62] no convincing changes of proton signals were observed when *R*-NA-Cys was added into LMV solution (Figure 7E), compared with their original status (Figure 7C for *R*(*S*)-NA-Cys; Figure 7D for LMV). By contrast, the addition of *S*-NA-Cys induced obvious chemical shifts of all proton signals for amides (red dashed circles), and proton-coupling and overlaps between the chiral protons of LMV (green dashed circles) and amide groups in *S*-NA-Cys (blue dashed circles) were observed (Figure 7F). All these data clearly demonstrate that LMV has much stronger binding with *S*-NA-Cys than *R*-NA-Cys. Besides that, Phe−Phe is also recognized as another important sequence contributing to protein amyloidosis.[67,68] Similar chiral discrimination effect was also observed between *R*- and *S*-NA-Cys when they interacted with Val-Phe-Phe (residues 18−20 in Aβ(1−40)) (see Figure S13 and S14 in Supporting Information). Such stereoselective interactions between binding sites of Aβ(1−40) and *R*(*S*)-Cys moieties may directly contribute to the different effect of *R*(*S*)-Cys-GO on amyloid formation.

3. CONCLUSIONS

Here we used chiral-modified GO as a platform to study the chiral effect for amyloid formation on surfaces. We found that surface chirality strongly influences the conformational transition from α-helix to β-sheet, the adsorption of monomers and oligomers, and the subsequent fibrillation process. On the one hand, the stereoselective interaction between chiral moieties on surface and Aβ peptides is the origin of this chiral effect, while surface can highly enrich oligomers,[69] which make the effect visible. On the other hand, the synergy between the chiral interaction and surface requires that the distance between them should be short enough; otherwise the surface may not be

dx.doi.org/10.1021/ja5049626 | J. Am. Chem. Soc. 2014, 136, 10736−10742

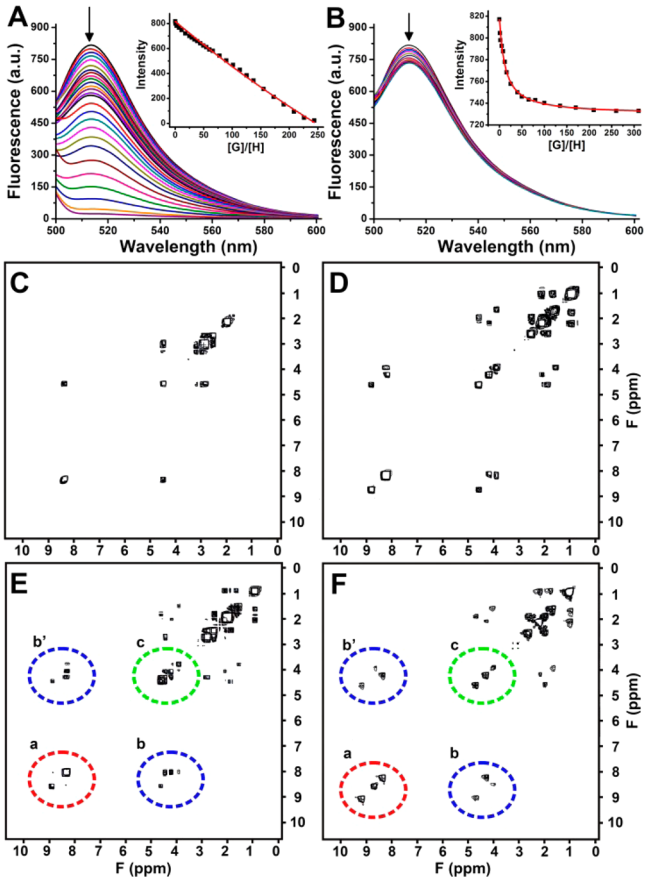

Figure 7. (A, B) Fluorescence spectra of fluorescein-labeled Leu-Met-Val (LMV) upon addition of various amounts of *R*-NA-Cys (A) or *S*-NA-Cys (B) in Tris-buffer solution (pH 7.4, 1 mM) at 25 °C. The insets show the relationship between fluorescent intensity and molar ratios of *R*-(*S*)-NA-Cys and LMV. (C–F) 2D ^{1}H–^{1}H COSY NMR spectra of racemic *R*(*S*)-NA-Cys (C), LMV (D), and mixtures of LMV (4×10^{-3} mol·L^{-1}) with equivmolar amounts of *R*-NA-Cys (E), or with *S*-NA-Cys (F) in d_6-DMSO. Detailed active proton assignments (amides and chiral protons indicated by color circles) are shown in Figure S17 in Supporting Information.

able to participate into the process. These results provide interesting insights at least from one aspect to comprehensively understand the crucial roles of biological membranes on protein amyloidosis, and how their intrinsic properties contribute to this process.[70,71] Besides that, it also points to a prospect for broad application of GO in biology and medicine[72,73] if chiral elements[74,75] are converged.

■ ASSOCIATED CONTENT

Supporting Information

Experimental details for synthesis of chiral cysteine modified GO, peptide preparation, ThT fluorescence spectroscopy, AFM, QCM adsorption, ITC, CD spectroscopy, and fluorescence titration, characterization data of GO samples, dynamic growth curves of Aβ(1–40) peptides incubated with various *R*(*S*)-cysteine derivatives or *R*(*S*)-serine or -tyrosine modified GO at 37 °C, AFM images of peptide oligomers, QCM adsorption curves of peptides adsorbed on quartz crystals modified with *R*- or *S*-cysteine, time-dependence of CD spectral changes of Aβ(1–40) peptides during fibrillogenesis, investigation of intermolecular interaction between VFF, LMV, and various *R*(*S*)-cysteine derivatives, one-dimensional ^{1}H NMR spectra of LMV or VFF interacted with equimolar amounts of *R*(*S*)-NA-Cys. This material is available free of charge via the Internet at http://pubs.acs.org.

■ AUTHOR INFORMATION

Corresponding Authors

suntl@whut.edu.cn

qing@whut.edu.cn

Notes

The authors declare no competing financial interest.

■ ACKNOWLEDGMENTS

We thank the National Natural Science Foundation of China (Grants 21104061, 21275114, 91127027, and 51173142), the China National Funds for Distinguished Young Scientists (Grant 51325302), the Major State Basic Research Development Program of China (973 Program, Grant 2013CB933002), and the Program of Introducing Talents of Discipline to Universities (Grant B13035) for funding support. G. Qing acknowledges Hubei Provincial Department of Education for financial assistance through the "Chutian Scholar" program, and Scientific Research Foundation for the Returned Overseas Chinese Scholars, State Education Ministry. We also thank Dr. X. J. Wu for his help in the analysis of ^{1}H–^{1}H COSY NMR spectra.

■ REFERENCES

(1) Chiti, F.; Dobson, C. M. *Annu. Rev. Biochem.* **2006**, *75*, 333.
(2) Dobson, C. M. *Nature* **2003**, *426*, 884.
(3) Soto, C. *Nat. Rev. Neurosci.* **2003**, *4*, 49.
(4) Selkoe, D. J. *Physiol. Rev.* **2001**, *81*, 741.
(5) Hamley, I. W. *Nat. Chem.* **2010**, *2*, 707.
(6) Moores, B.; Drolle, E.; Attwood, S. J.; Simons, J.; Leonenko, Z. *PLoS One* **2011**, *6*, No. e25954.
(7) Deng, Y.; Zhu, X. Y.; Kienlen, T.; Guo, A. *J. Am. Chem. Soc.* **2006**, *128*, 2768.
(8) Chi, E. Y.; Frey, S. L.; Winans, A.; Lam, K. L. H.; Kjaer, K.; Majewski, J.; Lee, K. Y. C. *Biophys. J.* **2010**, *98*, 2299.
(9) Garland, A.; Shen, L.; Zhu, X. Y. *Prog. Surf. Sci.* **2012**, *87*, 1.
(10) Shen, L.; Adachi, T.; Bout, D. V.; Zhu, X. Y. *J. Am. Chem. Soc.* **2012**, *134*, 14172.
(11) Narayan, P.; Ganzinger, K. A.; McColl, J.; Weimann, L.; Meehan, S.; Qamar, S.; Carver, J. A.; Wilson, M. R.; St. George-Hyslop, P.; Dobson, C. M.; Klenerman, D. *J. Am. Chem. Soc.* **2013**, *135*, 1491.
(12) Butterfield, S. M.; Lashuel, H. A. *Angew. Chem., Int. Ed.* **2010**, *49*, 5628.
(13) Berthelot, K.; Cullin, C.; Lecomte, S. *Biochimie* **2013**, *95*, 12.
(14) Burke, K. A.; Yates, E. A.; Legleiter, J. *Front. Neurol.* **2013**, *4*, 1.
(15) Aisenbrey, C.; Borowik, T.; Byström, R.; Bokvist, M.; Lindström, F.; Misiak, H.; Sani, M.-A.; Gröbner, G. *Eur. Biophys. J.* **2008**, *37*, 247.
(16) Evangelisti, E.; Cecchi, C.; Cascella, R.; Sgromo, C.; Becatti, M.; Dobson, C. M.; Chiti, F.; Stefani, M. *J. Cell Sci.* **2012**, *125*, 2416.
(17) Matsuzaki, K. *Biochim. Biophys. Acta* **2007**, *1768*, 1935.
(18) Tofoleanu, F.; Buchete, N.-V. *Prion* **2012**, *6*, 339.
(19) Vestergaard, M. C.; Morita, M.; Hamada, T.; Takagi, M. *Biochim. Biophys. Acta* **2013**, *1828*, 1314.
(20) Luckey, M. In *Membrane Structural Biology with Biochemical and Biophysical Foundations*; Cambridge University Press: Cambridge, U.K., 2008.
(21) Finefield, J. M.; Sherman, D. H.; Kreitman, M.; Williams, R. M. *Angew. Chem., Int. Ed.* **2012**, *51*, 4802.
(22) Ernst, K.-H. *Phys. Status Solidi B* **2012**, *249*, 2057.
(23) Zhang, M. X.; Qing, G. Y.; Sun, T. L. *Chem. Soc. Rev.* **2012**, *41*, 1972.

(24) Wang, X.; Gan, H.; Sun, T. L. *Adv. Funct. Mater.* **2011**, *21*, 3276.
(25) Bandyopadhyay, D.; Prashar, D.; Luk, Y.-Y. *Langmuir* **2011**, *27*, 6124.
(26) Geva, M.; Frolow, F.; Eisenstein, M.; Addadi, L. *J. Am. Chem. Soc.* **2003**, *125*, 696.
(27) Sun, T. L.; Han, D.; Rhemann, K.; Chi, L. F.; Fuchs, H. *J. Am. Chem. Soc.* **2007**, *129*, 1496.
(28) Li, Z.; Köwitsch, A.; Zhou, G. Y.; Groth, T.; Fuhrmann, B.; Niepel, M.; Amado, E.; Kressler, J. *Adv. Healthcare Mater.* **2013**, *2*, 1377.
(29) Jariwala, D.; Sangwan, V. K.; Lauhon, L. J.; Marks, T. J.; Hersam, M. C. *Chem. Soc. Rev.* **2013**, *42*, 2824.
(30) Novoselov, K. S.; Faĺko, V. I.; Colombo, L.; Gellert, P. R.; Schwab, M. G.; Kim, K. *Nature* **2012**, *490*, 192.
(31) Cote, L. J.; Kim, J.; Tung, V. C.; Luo, J. Y.; Kim, F.; Huang, J. X. *Pure Appl. Chem.* **2011**, *83*, 95.
(32) Kim, J.; Cote, L. J.; Kim, F.; Yuan, W.; Shull, K. R.; Huang, J. X. *J. Am. Chem. Soc.* **2010**, *132*, 8180.
(33) Hoff, D.; Sheikh, L.; Bhattacharya, S.; Nayar, S.; Webster, T. J. *Int. J. Nanomed.* **2013**, *8*, 703.
(34) Liu, G. D.; Shen, H.; Mao, J. N.; Zhang, L. M.; Jiang, Z.; Sun, T.; Lan, Q.; Zhang, Z. J. *ACS Appl. Mater. Interfaces* **2013**, *5*, 6906.
(35) Weidenfeller, C.; Schrot, S.; Zozulya, A.; Galla, H.-J. *Brain Res.* **2005**, *1053*, 162.
(36) Pumera, M. *Mater. Today* **2011**, *14*, 308.
(37) Yang, K.; Feng, L. Z.; Shi, X. Z.; Liu, Z. *Chem. Soc. Rev.* **2013**, *42*, 530.
(38) Mahmoudi, M.; Akhavan, O.; Ghavami, M.; Rezaee, F.; Ghiasi, S. M. A. *Nanoscale* **2012**, *4*, 7322.
(39) Yu, X.; Wang, Q. M.; Lin, Y. A.; Zhao, J.; Zhao, C.; Zheng, J. *Langmuir* **2012**, *28*, 6595.
(40) Chua, C. K.; Pumera, M. *Chem. Soc. Rev.* **2013**, *42*, 3222.
(41) Wu, D. Q.; Zhang, F.; Liang, H. W.; Feng, X. L. *Chem. Soc. Rev.* **2012**, *41*, 6160.
(42) Li, M.; Yang, X. J.; Ren, J. S.; Qu, K. G.; Qu, X. G. *Adv. Mater.* **2012**, *24*, 1722.
(43) Kumar, S.; Walter, J. *Aging* **2011**, *3*, 803.
(44) Hortschansky, P.; Schroeckh, V.; Christopeit, T.; Zandomeneghi, G.; Fändrich, M. *Protein Sci.* **2005**, *14*, 1753.
(45) Hellstrand, E.; Boland, B.; Walsh, D. M.; Linse, S. *ACS Chem. Neurosci.* **2010**, *1*, 13.
(46) Cao, P.; Raleigh, D. P. *Biochemistry* **2012**, *51*, 2670.
(47) Bartolini, M.; Naldi, M.; Fiori, J.; Valle, F.; Biscarini, F.; Nicolau, D. V.; Andrisano, V. *Anal. Biochem.* **2011**, *414*, 215.
(48) LeVine, H. *Protein Sci.* **1993**, *2*, 404.
(49) Kowalewski, T.; Holtzman, D. M. *Proc. Natl. Acad. Sci. U. S. A.* **1999**, *96*, 3688.
(50) Liu, G.; Zhang, G. In *QCM-D Studies on Polymer Behavior at Interfaces*; Springer Heidelberg: New York, 2013.
(51) Kotarek, J. A.; Johnson, K. C.; Moss, M. A. *Anal. Biochem.* **2008**, *378*, 15.
(52) Chen, W.-J.; Zhang, S.; Zhang, W.-G.; Fan, J.; Yin, X.; Zheng, S.-R.; Su, W.-C.; Zhang, Z.; Hong, T. *Chirality* **2012**, *24*, 804.
(53) Jelesarov, I.; Bosshard, H. R. *J. Mol. Recognit.* **1999**, *12*, 3.
(54) Tian, F. F.; Li, J. H.; Jiang, F. L.; Han, X. L.; Xiang, C.; Ge, Y. S.; Li, L. L.; Liu, Y. *RSC Adv.* **2012**, *2*, 501.
(55) Shval, A.; Mastai, Y. *Chem. Commun.* **2011**, *47*, 5735.
(56) de Bruin, T. J. M.; Marcelis, A. T. M.; Zuilhof, H.; Sudhölter, E. J. R. *Langmuir* **2000**, *16*, 8270.
(57) Fu, L.; Liu, J.; Yan, E. C. Y. *J. Am. Chem. Soc.* **2011**, *133*, 8094.
(58) Terzi, E.; Hölzemann, G.; Seelig, J. *J. Mol. Biol.* **1995**, *252*, 633.
(59) Bokvist, M.; Lindström, F.; Watts, A.; Gröbner, G. *J. Mol. Biol.* **2004**, *335*, 1039.
(60) Fezoui, Y.; Hartley, D. M.; Harper, J. D.; Khurana, R.; Walsh, D. M.; Condron, M. M.; Selkoe, D. J.; Lansbury, P. T., Jr.; Fink, A. L.; Teplow, D. B. *Amyloid: Int. J. Exp. Clin. Invest.* **2000**, *7*, 166.
(61) Petkova, A. T.; Yau, W.-M.; Tycko, R. *Biochemistry* **2006**, *45*, 498.
(62) Paravastu, A. K.; Leapman, R. D.; Yau, W.-M.; Tycko, R. *Proc. Natl. Acad. Sci. U.S.A.* **2008**, *105*, 18349.
(63) Bertini, I.; Gonnelli, L.; Luchinat, C.; Mao, J. F.; Nesi, A. *J. Am. Chem. Soc.* **2011**, *133*, 16013.
(64) Sievers, S. A.; Karanicolas, J.; Chang, H. W.; Zhao, A.; Jiang, L.; Zirafi, O.; Stevens, J. T.; Münch, J.; Baker, D.; Eisenberg, D. *Nature* **2011**, *475*, 96.
(65) Pu, L. *Chem. Rev.* **2004**, *104*, 1687.
(66) Gale, P. A.; García-Garrido, S. E.; Garric. *J. Chem. Soc. Rev.* **2008**, *37*, 151.
(67) Hilbich, C.; Kisters-woike, B.; Reed, J.; Masters, C. L.; Beyreuther, K. *J. Mol. Biol.* **1992**, *228*, 460.
(68) Tjernberg, L. O.; Näslund, J.; Lindqvist, F.; Johansson, J.; Karlström, A. R.; Thyberg, J.; Terenius, L.; Nordstedt, C. *J. Biol. Chem.* **1996**, *271*, 8545.
(69) Campioni, S.; Carret, G.; Jordens, S.; Nicoud, L.; Mezzenga, R.; Riek, R. *J. Am. Chem. Soc.* **2014**, *136*, 2866.
(70) Nel, A. E.; Mädler, L.; Velegol, D.; Xia, T.; Hoek, E. M. V.; Somasundaran, P.; Klaessig, F.; Castranova, V.; Thompson, M. *Nat. Mater.* **2009**, *8*, 543.
(71) Hamley, I. W. *Chem. Rev.* **2012**, *112*, 5147.
(72) Langer, R. *Science* **2001**, *293*, 58.
(73) Sharp, P. A.; Langer, R. *Science* **2011**, *333*, 527.
(74) Zepik, H.; Shavit, E.; Tang, M.; Jensen, T. R.; Kjaer, K.; Bolbach, G.; Leiserowitz, L.; Weissbuch, I.; Lahav, M. *Science* **2002**, *295*, 1266.
(75) Gellman, A. J. Enantioselectivity on Naturally Chiral Metal Surfaces. In *Model Systems in Catalysis: Single Crystals to Supported Enzyme Mimics*; Rioux, R. M., Ed.; Springer: New York, 2010.